



Efficacy of Delta-Tab in Controlling the Mixing Characteristics of Mach 1.8 Jet

B. Mahabir, P. Bhale and M. Kaushik[†]

Indian Institute of Technology, Kharagpur, West Bengal-721302, India

[†]Corresponding Author Email: mkaushik@aero.iitkgp.ac.in

(Received May 11, 2020; accepted September 24, 2020)

ABSTRACT

This present investigation inspects the mixing promoting the efficacy of two short delta tabs which is axis-symmetric, mounted circumferentially antipodal at the end for a Mach number 1.8 convergent-divergent circular nozzle computationally with the nozzle pressure ratios (NPRs) ranging from 4 to 8 with a unit step of one that covers all the critical states of the jet i.e., the overexpanded, the correctly-expanded and the underexpanded states of the jet. In order to minimize thrust loss, the geometric blockage offered by each delta tab is kept within 2.5%. The computational assessment is conducted by adopting and employing ANSYS-FLUENT which is a comprehensive engineering simulation software. Further, the entire steady flow computations are carried out on a three-dimensional numerical enclosure by implementing Reynolds-averaged Navier-Stokes equations along with the $\kappa - \omega$ shear stress transport turbulence model. Interestingly, vital plots including the centerline pressure decay as well as the pressure profiles are depicted for uncontrolled and controlled jets accordingly. Also, numerically obtained schlieren illustrations are adopted for visualization of the shock cell structure, expansion fan, and the Mach wave structure existing in the stream field. Furthermore, Mach variations are also depicted for the varied nozzle pressure ratios in the form of contours. The shock-strength, shock-length, and the progressive disparity found in the shock structures are reasonably demonstrated by the Mach contours. The results of this research are discovered to be in sensible concurrence with the earlier established exploratory results. A maximum core length reduction of 70.81% is observed in underexpanded condition at the nozzle pressure ratio of 6. Absorbingly, a controlled jet has been seen to get split in equal proportion along the succeeding direction of the nozzle exit at a distance of approximately $5D_e$, D_e indicating the exit diameter of the nozzle. Moreover, it was appealing to detect the development of jet dispersion along the succeeding direction of the nozzle exit periphery. The short delta tabs also performed satisfactorily in diminishing the waves and reducing the shock cell length as depicted via numerical schlieren images.

Keywords: Centerline pressure decay; Jet mixing; Core length; Mach contours; Numerical Schlieren; RANS; Mach number.

NOMENCLATURE

D_e	nozzle exit diameter	q	source term per unit mass
e	internal energy	\mathbf{V}	velocity vector
f	body force		
K	thermal conductivity	κ	turbulent kinetic energy
M	Mach number	ρ	density of fluid
P_b	back pressure	τ	shear stress
P_e	nozzle exit pressure	ω	dissipation of turbulent kinetic energy

1. INTRODUCTION

The mixing behaviour of a supersonic jet is a significant field of examination because of its wide applications like high-speed regimes such as in thrust augmentation, infra-red plume reduction, noise suppression, etc. Diverse preferences of supersonic

jets make them indispensable in the high-speed military and traveler airplanes. Simultaneously, different control procedures to advance jet blending attract the consideration of a few researchers to expand their beneficent accomplishments in particular fields. A number of researchers have reported numerous ways to enhance the extent of jet

mixing as can be found in the open literature. The enhancement can be done by either active or passive flow control methods. In active control, energized actuators are used to dynamically manipulate the flow, whereas, in passive control, geometrical modifications of some sort are employed. In recent years, a number of researchers have focussed their attention on employing geometrical alterations at the exit of the nozzle as the prominent passive control technique, such as implementing a short structural protrusion to the flow. This structural protrusion can be in the form of a tab that produces counter-rotating vortex pair thereby significantly affecting the mixing behaviour. From the concept of vortex dynamics, it can be stated that, if a tab generates vortices of diverse size with the behavior to transport mass, it would significantly improve the jet blending. Likewise, a couple of oppositely-rotating vortical shapes of mixed size is shedding from a triangular tab with larger vortices towards the base and smaller vortices towards the tip, as depicted in Fig. 1.

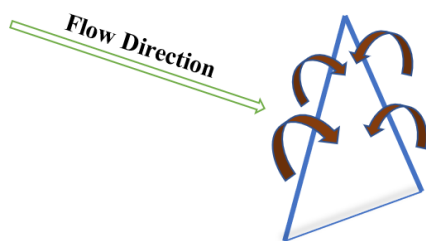


Fig. 1. Illustration of the vortex shedding from the triangular tab.

Furthermore, large-scaled vortices are effective suction generators and thus, helpful in inundating the ambient fluid into the jet flow field. This step of drawing the surrounding fluid mass towards the jet core is known as entrainment and only viscosity is the real cause of true entrainment via diffusion (Hussain, 1986). The large-sized vortices get fragmented into smaller vortices, in adhere to the law of conservation of momentum. It is an established fact that the appropriate ratio of larger vortices and smaller vortices induce influential mixing. In jet research, detection of this exact ratio in a turbulence dominated field is a problematic task. For researchers, measuring the decay in jet centerline pressure is a popular means for finding the appropriate proportion. The swifter the droop, the hastier is the mixing of the engulfed fluid mass with the jet field (Kaushik, 2019). A number of researchers have performed experimental research and analysis on jet mixing in the past and recent years. Bradbury and Khadem (1975) observed the factors like boundary-layer thickness at the nozzle, turbulence, and convergence had minimal impact on the outgrowth of a jet, in contrast, the introduction of small perturbation in the flow field like tabs, profoundly affect the jet development. The blending accentuation of heated and unheated jets along with subsonic and underexpanded supersonic jets by the introduction of mechanical obstructions, such as tabs, is confirmed in the

literature of Ahuja and Brown (1989). Further, Samimy *et al.* (1991) found that tabs employment induce vortices of streamwise nature into the flow field that increased the jet expansion substantially. Furthermore, relying on the geometry of the nozzle and tab placement, the stretching out of a jet can be either escalated or de-escalated accordingly. Considering those aspects, many studies have been carried out by deploying tabs of different geometries at the nozzle exit location. However, it is a known fact that jet mixing is enhanced by the production of mixed size vortices, shedding by the tab of varying half-width deployed at the nozzle exit. Considering those aspects, the present investigation specifically concentrates the efficacy of the delta tab in generating the mixing promoting vortices. In view of this, Zaman *et al.* (1992, 1993) concluded that the tabs weaken the expansion structure (shock) drastically and the impact of delta-tabs is more prominent when they are mounted circumferentially antipodal at the nozzle outlet resulting in enhanced mixing. Later, Behrouzi and McGuirk (2006) investigated the immediate-field mixing characteristics of nozzle stream controlled by delta tabs at each subsonic and supersonic conditions. They studied the impact of distinct tab specifications on the improvement of jet mixing. It is important to note that the descent of jet core speed feebly relies on the tab shape and tab inclination angle. Moreover, the optimum number of tabs is estimated as two. Beyond this limit, the efficiency of tabs decreases since the interaction of vortices with each other to a higher extent reduces their strength. Interestingly, Kaushik and Rathakrishnan (2013, 2015) declared that the strength as well as the size of vortices, shed by a controlled tab, and geometric modifications can improve it. Moreover, the strength of the vortices generated from a tab can be influenced through the corrugated shape deployed over tab geometries along with the implementation of sharp corners around the tab sharp boundary. Recently, in an experimental study, Thillaikumar *et al.* (2020) stated that, with the insertion of a tab in the diverging portion of a supersonic nozzle alters shock-cell appearance, which in turn abates the jet-core length of the corresponding supersonic jet. The aforementioned studies clearly reveal that the deployment of tabs with different structures over the supersonic nozzle effectively manipulates the shock cell structure in order to promote the supersonic jet mixing. Along with the experimental investigations, several computational studies also gained prominence owing to their economic advantages in predicting the jet mixing process. The Reynolds-Averaged Navier-Stokes (RANS) equation in anticipating the supersonic jet flows are well discussed in the review literature of Kaushik *et al.* (2015). They concluded that the RANS model is a conventional, relatively inexpensive but effective method in order to anticipate the supersonic jet core length along with the descent rate accurately. RANS two-equation model such as standard $\kappa - \epsilon$, realizable $\kappa - \epsilon$, $\kappa - \omega$ shear stress transport, etc. are widely used in engineering applications to predict the free

shear flows like jets. Launder *et al.* (1974) worked on the advancement of $\kappa - \epsilon$ turbulence model, where two differential equations namely the turbulent energy (κ) equation and the dissipation rate of turbulence energy (ϵ) equation are solved. Later, Pope (1978) stated a correction factor with the purpose of predicting the elongation in the jet potential core length accurately for the standard $\kappa - \epsilon$ turbulence model. Further, the computational analysis is conducted by Steffen *et al.* (1997) with a DTNS3D solver, which uses the eddy viscosity model based on Pope's $\kappa - \epsilon$ model. The results of the DTNS3D code for the delta tab controlled nozzle indicated sensible consent between the exploratory and the computational findings. It has been seen, vortex-generators are also widely used to improve the aerodynamics performance of giant wind turbines. Recently, Acarer (2020) confirmed that passive control methods possess, an advantage of the high value of coefficients of lift and drag. so, the passive method is more effective than the active method. Further, Ebrahimi and Movahhedi (2018), computationally inspected the impact of micro tabs and found that the output power of wind turbine improved due to the installation of micro tabs. Wang *et al.* (2017), discussed momentum transfer and vortex trajectory due to vortex generator computationally by the use of shear stress transport $\kappa - \omega$ turbulence model, found the vortex promoters can improve the coefficient of lift and can control flow separation. Also, for the compressible flow stream of Mach number 0.9, Tide and Babu (2008) stated that the shear stress transport k- ω turbulence model can predict the mean, turbulence quantities along with the prevailing tendencies in acoustic quantities with reasonable accuracy, which is better than the Wilcox k- ω model. Furthermore, Gross *et al.* (2010) performed correction in the turbulence model for supersonic stream by the application of overflow code along with different turbulence models and it was observed that the SST model performed better out of all the other models. Moreover, the k- ω and Spalart-Allmaras models were too diffusive, whereas the Baldwin-Barth model suppressed the mixing effect exorbitantly. Chin *et al.* (2013) proposed a numerical model to predict the stream behaviour in supersonic flow and impinging jet streams using both $\kappa - \omega$ SST and k- ϵ model and validated the findings with experimental results. It was observed that both these models accurately predict the shock formation inside the core region. Subsequently, Medeiros *et al.* (2014) performed simulations on supersonic flow to compare large eddy simulation including unsteady RANS and compared it with RANS $\kappa - \omega$ shear stress transport turbulence models. It was noticed, that the results obtained with SST $\kappa - \omega$ model presented a preferable consent with the data obtained experimentally as compared with other models. Particularly, the pressure profile which shows an identical pattern with the experimental results was obtained with shear stress transport $\kappa - \omega$ turbulence model. Essentially, it is evident from the above observations, that the

numerical investigation on the supersonic stream regulated with the delta tabs has not been investigated extensively. Hence, the work presented here deals with the computational assessment of supersonic jet, controlled with short delta tabs mounted on the outlet periphery of a three-dimensional convergent-divergent nozzle designed for Mach number 1.8 and the numerical calculations were carried out on a comprehensive engineering simulation software ANSYS FLUENT 16.0. A short delta tab involves two sharp edges and these edges are responsible for inducing mixed sized vortices resulting in enhanced mixing. It has been observed, that for most of the jet studies, the preferred turbulence model adopted was $\kappa - \epsilon$, because of its suitability in free shear flow regions and better predictions away from the wall. However, in the present investigation, the controlled jet is discussed which involves wall effect arising near the tabs and it is well known that the $\kappa - \omega$ model is best suited to capture these wall effects. In other words, the present computational assessment demands a model that is suitable for both free shear flow as well as obstructed flow and the $\kappa - \omega$ shear stress transport turbulence model satisfies this requirement. Therefore, the turbulence model adopted to carry out the simulations in this study involved the RANS (Reynolds-averaged Navier-stokes) model including the $\kappa - \omega$ shear stress transport model. Recently, Ranjan *et al.* (2020) performed a numerical study on passive control of supersonic jet by adopting the $\kappa - \omega$ shear stress transport model and they observed quite satisfactory results. Likewise, the implementation of the $\kappa - \omega$ shear stress transport model was concluded suitable for present computational assessment. Going forward, simulated outcomes were formulated into decisive plots, like descend of centerline pressure along with pressure profiles, for each case of unconstrained and constrained jets. In addition to this, numerical schlieren images are adopted for apparent visualization of shock-structures, expansion fan, and the Mach wave frame existing in the core of the jet flow. Also, contours indicating Mach variations are depicted for different nozzle pressure ratios of 4, 5, 6, 7, and 8. The findings of this assessment are found to be explicitly allied with the earlier established results, which is plausible. A maximum core length reduction of 70.81% is detected in underexpanded conditions at a nozzle pressure of 6. It is plausible to find, controlled jet had been seen split up along the downstream of the nozzle outlet at the length of nearly around 5 De. Also, it is interesting to observe the development of jet spread downstream of the nozzle outlet periphery. It is fair enough to say, that short delta tabs performed effectively in abating the waves and contraction of shock-cell length as illustrated via numerical schlieren illustrations. Eventually, numerical results effectively predict the decay of centerline pressure, jet spreading rate, and shock cell formation inside of the stream, which strongly indicates enhanced mixing due to the deployment of delta tabs

2. COMPUTATIONAL METHODOLOGY

2.1 Geometric Model and Flow Domain

A 3D model of a Convergent-divergent nozzle, with diametrically opposite delta tabs at its periphery, is generated, as shown in Fig. 2. The entire design parameters for the nozzle are determined by using area-Mach number relations. The nozzle inlet diameter is taken as 30 mm with the throat diameter to be 20 mm. The divergence angle is 7° with an area ratio of 1.438 which is suitable for Mach number 1.8 with a nozzle exit diameter of 23.99 mm. The dimensions of both delta tabs are selected in such a manner that they offer a blockage ratio below 5% in order to reduce the thrust loss due to blockage. In order to capture the shock-cells generated along the jet core, this three-dimensional nozzle is placed inside a cylindrical domain enclosure as illustrated in Fig. 3. Also, the axial length of enclosure is taken as $30D_e$ because the flow velocity beyond that attains a self-similar behaviour whereas in the transverse direction it is taken as $5D_e$ after which the study of flow will be insignificant.

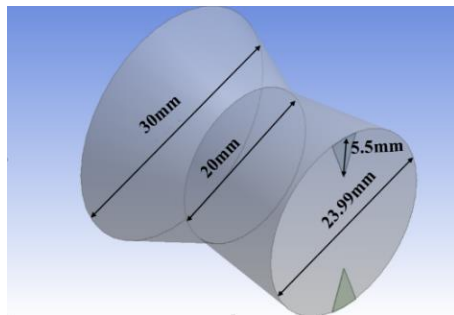


Fig. 2. Geometric model of a nozzle with delta tabs at the outlet.

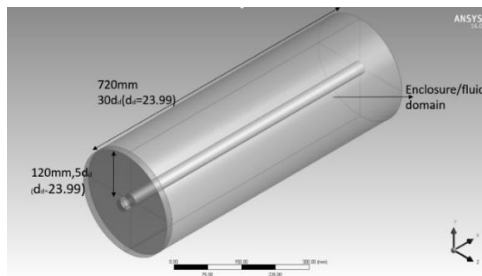


Fig. 3. Flow domain.

2.2 Governing Equations

The conservative form of continuity, momentum, and energy equations are used in the present numerical simulation as the governing equations for programming convenience.

2.3 Turbulence Model

The Reynolds-Averaged Navier–Stokes (RANS) model is the most common and widely accepted turbulent model to computationally investigate the flow field. The computations with the RANS model

are essentially restricted to the average turbulent flows while ignoring the turbulent fluctuations. Notice that, unlike incompressible flows, the averaging process of the compressible flows emerges with a product of the fluctuating density and the velocity or internal energy terms. Therefore, Favre (1969) extended the idea of compressible Reynolds-averaged Navier-Stokes equations by rewriting the compressible turbulent equations in terms of the density-weighted variables. The study concluded that the flow field variables decompositions in terms of density-weighted are the best choice due to their superior accuracy than the mass-weighted variables (Hirsch, 1990; Gatski and Bonnet, 2009). The RANS equations for the compressible flows are as follows:

$$\frac{\partial(\overline{\rho u_j})}{\partial x_j} = 0 \quad (1)$$

$$\frac{\partial(\overline{u_j \rho u_i})}{\partial x_j} = -\frac{\partial p}{\partial x_i} + \frac{\partial \overline{\sigma_{ij}}}{\partial x_j} + \frac{\partial \overline{\tau_{ij}}}{\partial x_j} \quad (2)$$

$$\frac{\partial(\overline{u_j \rho \hat{H}})}{\partial x_j} = \frac{\partial}{\partial x_j} (\overline{\sigma_{ij} u_i} + \overline{\sigma_{ij} \hat{u}_i}) - \frac{\partial}{\partial x_j} (\overline{q_j} + c_p \overline{\rho \hat{u}_j T} - \overline{u_i \tau_{ij}} + \frac{1}{2} \overline{\rho \hat{u}_i \hat{u}_i \hat{u}_j}) \quad (3)$$

Where, $\hat{H} = \hat{E} + \frac{p}{\rho}$; and $\overline{q_j} = -K_T \frac{\partial T}{\partial x_j}$

E = Internal energy.

K_T = Thermal conductivity.

$\overline{\sigma_{ij}}$ is represented as viscous stress tensor. In addition, the term $-\overline{\rho \hat{u}_i \hat{u}_j}$ represents the Reynold stress (τ_{ij}) in Eq. 2.

Notice that, the cap over the dependent variables (for example, f) denotes the density-weighted value such as,

$$\hat{f} = \frac{\overline{\rho f}}{\overline{\rho}}; f = \hat{f} + \tilde{f}, \text{ and } \overline{\rho \tilde{f}} = 0$$

In this manner, the product of density fluctuation and the other fluctuating quantities will be removed.

In the present computational analysis, the closure of the RANS equation is achieved by the shear stress transport $\kappa - \omega$ model. This (SST) $\kappa - \omega$ turbulence model has the advantage that it implements the $\kappa - \omega$ model in the near-wall region with free stream independence of $\kappa - \epsilon$ in the far-field region. Two prominent equations (Eq. 4 and 5) are used by this model to consider the effect of turbulence.

Transport equation for Turbulent Kinetic Energy

$$\frac{\partial}{\partial t} (\rho \kappa) + \frac{\partial}{\partial x_i} (\rho \kappa u_i) = \frac{\partial}{\partial x_j} \left(\alpha_\kappa \frac{\partial \kappa}{\partial x_j} \right) + G_\kappa - T_\kappa + S_\kappa \quad (4)$$

Transport equation for the rate of dissipation of Turbulent Kinetic Energy

$$\frac{\partial}{\partial t} (\rho \omega) + \frac{\partial}{\partial x_i} (\rho \omega u_i) = \frac{\partial}{\partial x_j} \left(\alpha_\omega \frac{\partial \omega}{\partial x_j} \right) + G_\omega - T_\omega + D_\omega + S_\omega \quad (5)$$

In the above equation, G_κ represents the turbulence kinetic energy generation because of the average

velocity gradients, whereas G_ω represents the dissipation rate generation. T_κ and T_ω denotes the diffusion of κ and ω owing to turbulence, S_κ and S_ω are the source terms. Also, the cross-diffusion term is represented by D_ω .

In the high Mach-number flow conditions, a phenomenon of dilatation dissipation is observed, which happens because of compressibility affecting turbulence. It is absent in case of incompressible flow. The selection of (SST) $\kappa - \omega$ model was based on the requirement of simultaneously computing the combined effect of high turbulence flow and low Reynolds number effect.

2.4 Meshing

In the present investigation, the computational model is discretized by the structural hexahedral mesh with almost 2.1 million grid size as illustrated in Fig. 4. The skewness for this mesh is kept about 0.5, which ensures the regular grid of perfect geometrical shape and there is a node to node connection for smooth simulation. Around the near-wall zone, y^+ value is found to be between 5 and 30. Furthermore, an alteration of around 5 to 10 μm is observed at the spacing in the near-wall analogous to the y^+ value of the wall. The mesh near the jet centreline starting from the nozzle inlet to the end of the enclosure along the downstream is kept extremely fine because, in this region, shocks need to be captured which helps in making the investigation computationally economical, as shown in Fig. 5.

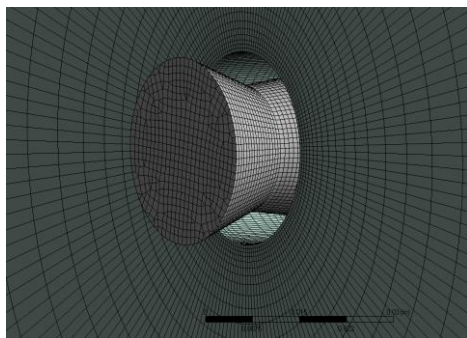


Fig. 4. Hexahedral mesh generation over the model.

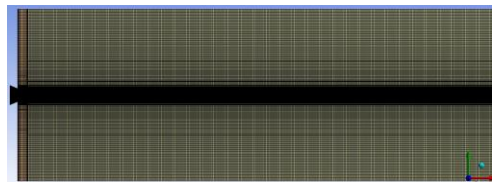


Fig. 5. Hexahedral structured mesh of the computational domain cut plane.

2.5 Boundary Conditions

For achieving an effective solution to any boundary value problem, some essential constraints are needed to be assigned. These constraints are known as boundary conditions. Since the flow is highly compressible and supersonic, a density-based steady-

state solver has been used. Depending on the nozzle exit diameter, the Reynolds numbers for Mach 1.8 jet at the nozzle outlet plane are 2.64×10^5 and 1.88×10^5 for NPR 4 and NPR 8, respectively. The boundary conditions associated with this numerical problem are depicted in Figs. 6(a), 6(b), 6(c), and 6(d), respectively. The shear stress transport $\kappa - \omega$ turbulence model is adopted because of its perfect behaviour in the adverse pressure conditions as well as its suitability with this model. This particular turbulence model is found to have compatibility in the flow separation situation. Air (ideal gas) is used by the solver as the working fluid and viscosity is Sutherland type. In fact, Sutherland's viscosity defines a relation between temperature and dynamic viscosity. It also gives more accurate results. The inlet section of the nozzle is considered as nozzle inlet and it is given pressure-inlet through which flow initiates (Fig. 6(a)). The outer surface of the convergent-divergent nozzle is chosen as nozzle-wall as shown in Fig. 6(b). The delta tabs at the outlet of the nozzle that interrupts the fluid flow are selected as well. Whereas, the cylindrical enclosure (far field) is given pressure inlet as illustrated in Fig. 6(c). The outer enclosure portion is given a pressure outlet as shown in Fig. 6(d).

Table 1 Boundary conditions

1	Nozzle inlet	Pressure Inlet
2	Nozzle wall	Wall
3	Delta Tabs	Wall
4	Far-field	Pressure Inlet
5	Enclosure outlet	Pressure Outlet

2.6 Grid Independence Test

As the grid size increases, the probability of achieving accuracy in the simulation will also be high. In the grid independence test (GIT) shown in Fig. 7, we find the optimum grid size above which the variation in the results will be almost negligible, and that optimum grid size for our model is found to be 2.1 million.

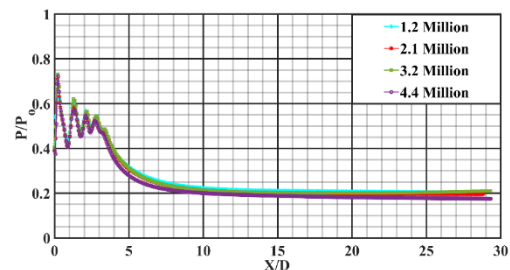
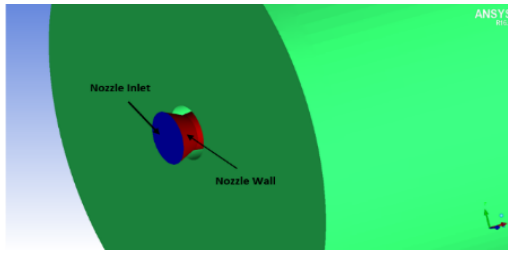
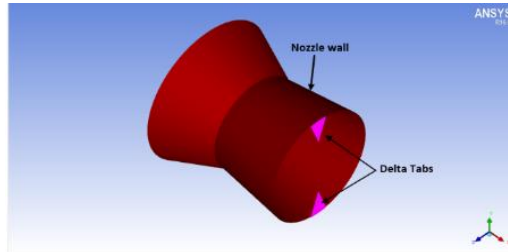


Fig. 7. Grid independency test.

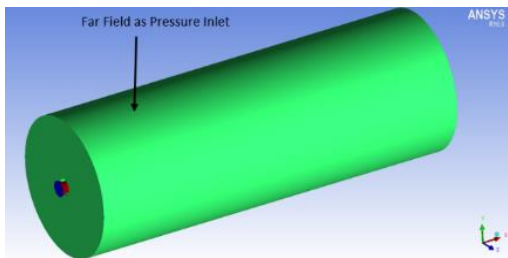
In the present study, we numerically performed the simulation for the grid sizes from 1.2 million to 4.4 million and we found 2.1 million grid size to be the best for numerical simulation which saved a lot of our computational time.



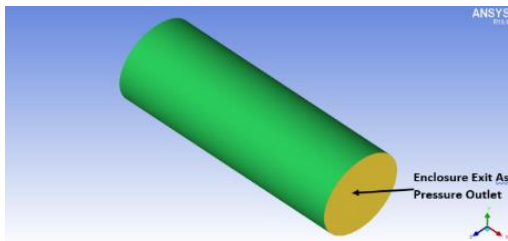
(a) Nozzle inlet as pressure inlet



(b) Nozzle and delta tab surface as wall



(c) Far-field as pressure inlet



(d) Enclosure outlet as pressure outlet

Fig. 6. Boundary conditions.

2.7 Validation

The numerically simulated results need to be verified after the final selection of the grid size. This validation is done by a diligent comparison of the numerical observations with the earlier established experimental results. The validation ensures the accuracy of the ongoing investigation. The present numerical result is validated with the result of [Maruthupandiyam and Rathakrishnan \(2018\)](#). From Fig. 8, it can be well observed that although there is a small variation in the Mach number of the numerical problem as compared to the experimental problem, the inlet expansion conditions are the same. Furthermore, for moderate supersonic flows, the effects of expansion condition dominate the flow compared to a small variation in the Mach number. The investigated numerical results are thus found to have a significant coherence with the established experimental results.

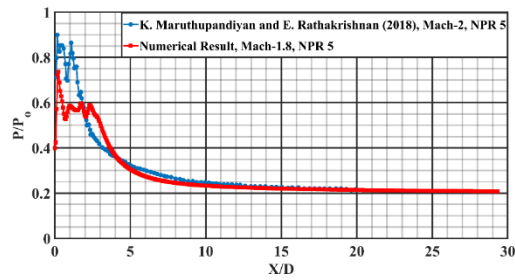


Fig. 8. Validation of the numerical analysis.

3 RESULTS AND DISCUSSION

The aim of this presented computational study is to investigate the effectiveness of diametrically opposite delta tabs in promoting the jet mixing, located at the outlet for a Mach number 1.8 supersonic nozzle, in the vicinity of adverse, zero, and favourable pressure gradient at the nozzle outlet. The estimation of the decay in centreline pressure along with radial pressure profile in the direction along and normal to the tabs are useful techniques in order to quantify the blending of a jet. On the other hand, the qualitative observations will be obtained by the computationally generated Mach contour and numerical schlieren images.

3.1 Centerline Pressure Decay

The variation in the non-dimensionalized total pressure with respect to the non-dimensionalized distance along the downstream-direction of the nozzle outlet is discussed with the centerline pressure decay plots, plotted for the case of both unconstrained and constrained jets, for different nozzle pressure ratios from 4 to 8 (Figs. 9 to 13). The centerline pressure decay plot is considered a well-established means for directly measuring the essential features such as core length of jet, characteristic decay, and strength of waves prevailing in the shock cell structure. The centerline pressure decay plots for the cases of unconstrained and constrained jets at NPR 4 with 36.40% of overexpansion is depicted in Fig. 9. Also, for the uncontrolled jet, total pressure oscillation within the supersonic core region can be clearly visualized in the plot of centerline pressure decay, indicating the successive evolution of the compression and the expansion waves. Essentially, supersonic jet core length is determined as the distance between the nozzle outlet and the axial downstream position up to which supersonic flow exists. Here, in the core of the uncontrolled supersonic stream, six prominent shock-cell structures are found, which can be clearly illustrated, however, are reduced to three shock cells in case of the controlled jet. Similarly, the supersonic jet core length elongates up to $X/D = 8.02$ for the uncontrolled jet, whereas by the introduction of delta tabs, the core length reduces up to $X/D = 2.58$. It has been observed that there is a decrement in the core length of 67.80 %.

Likewise, for NPR 5, centreline pressure decay is illustrated in Fig. 10. NPR 5 represents the case of

overexpansion by 20.50%. Absorbingly, the supersonic jet core length slightly expands with an increase in the corresponding NPR. Furthermore, the jet core length is found to be reduced by 69.03% when the delta tabs are introduced.

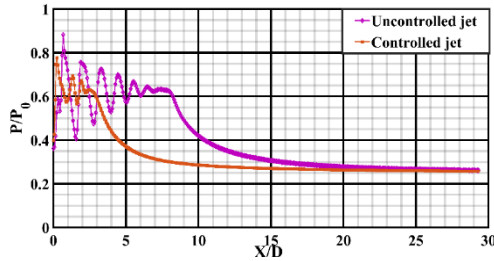


Fig. 9. C.P.D comparison for constrained and unconstrained jet at NPR 4.

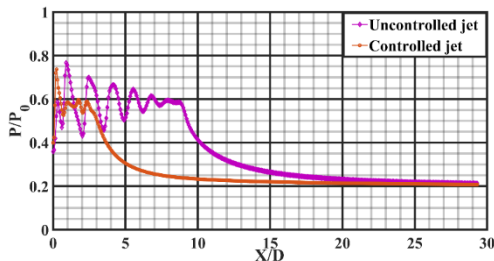


Fig. 10. C.P.D comparison for the constrained and unconstrained jet at NPR 5.

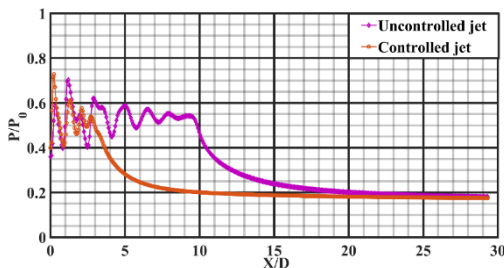


Fig. 11. C.P.D comparison for the constrained and unconstrained jet NPR 6.

Figure 11, represents the centreline pressure decay plot for controlled and as well as uncontrolled jets for the NPR 6 which is the condition of correct expansion of jet. When the NPR is increased to 6, the supersonic core length of about 9.67D was observed in the uncontrolled jet. However, by the deployment of delta tabs, there is a decrement of 2.82D in the jet core length. Further, the abatement in core length is calculated to be 70.81%, which is maximum at this particular NPR, indicating maximum mixing.

The centerline pressure decay of NPR 7, which is a case of underexpansion is illustrated in Fig. 12. The number of prominent shock-cells is found to be seven in the case of the uncontrolled jet. For the controlled condition of jets, the exact number of shock-cells is reduced to four. Likewise, the uncontrolled jet core elongates to about $X/D = 10.34$,

on the other side, for the controlled jet, the core length is observed as $X/D = 3.48$.

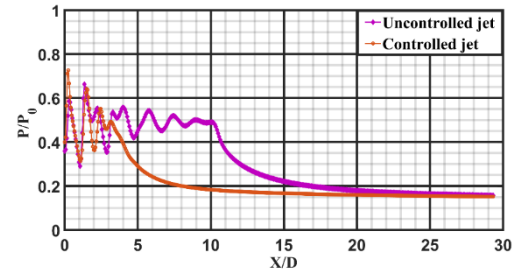


Fig. 12. C.P.D comparison for the constrained and unconstrained jet at NPR 7.

At NPR 8, which is a case of an underexpanded state, the outcomes are shown in Fig. 13. Here, the uncontrolled jet core length is observed as $X/D = 10.72$, and it shrinks to $X/D = 4.14$ for the controlled jet. The percentage of underexpansion at this NPR is found to be 27.18%.

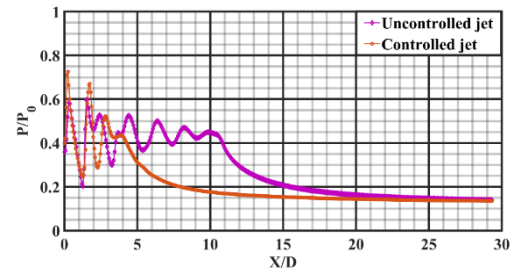


Fig. 13. C.P.D comparison for the constrained and unconstrained jet at NPR 8.

Certainly, percentage core length contraction is observed as 61.36% which is the minimum among all the NPRs. It indicates less mixing in underexpansion case. Accordingly, the study of centerline pressure decay for controlled and uncontrolled jet implies that delta tabs perform better for overexpanded state. Indeed, at NPR 6, which is nearly correct expansion level, the maximum core length reduction of about 70.81% was observed. This indicates the rapid decay of the centerline pressure along with faster jet mixing at this particular NPR for controlled conditions.

3.2 Percentage Length Reduction

The contraction found in the jet core along the streamwise direction for controlled jet directly specifies the efficacy of the delta tab in mixing enhancement. This shrinkage in the jet core length is presented here to express the extent of jet blending. The reduction in the percentage of jet core length is described as the ratio of the decrement in the length of the core due to deployment of the delta tab to the uncontrolled jet core length and it can be represented as,

$$(\text{Percentage Reduction in core length}) =$$

$$\left[\left(\frac{L_{\text{uncontrolled}} - L_{\text{controlled}}}{L_{\text{uncontrolled}}} \right) \times 100 \right]$$

In this present investigation, percentage core length reduction is obtained for every NPR ranging from 4 to 8 with the step of one and it is found that in controlled cases, delta tabs weaken the shocks which result in the decrement of jet core length. A larger reduction of jet core implies efficient mixing. The maximum percentage of decrement in jet core length was observed to be 70.81% at NPR 6, specifying maximum mixing enhancement, as shown in Table 2 and Fig. 14.

Table 2 Percentage reductions in jet core length for varied NPRs

NPR	$L_{\text{uncontrolled}}$	$L_{\text{controlled}}$	$\% \left(\frac{\Delta L}{L} \right)$
4	8D	2.5D	67.80
5	8.9D	2.7D	69.03
6	9.6D	2.8D	70.81
7	10.3D	3.4D	66.34
8	10.7D	4.1D	61.36

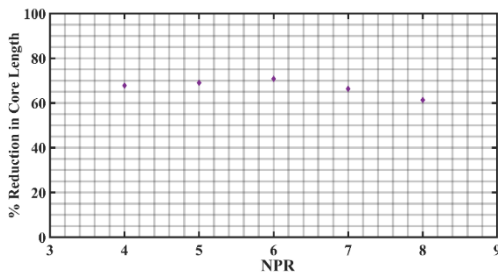


Fig. 14. Deviation of percentage decrement in jet core length at different NPRs.

3.3 Radial Pressure Profile

The pressure variation along the length of the delta tabs as well as along the width of the delta tabs for varying streamwise positions has been investigated for different sets of NPR.

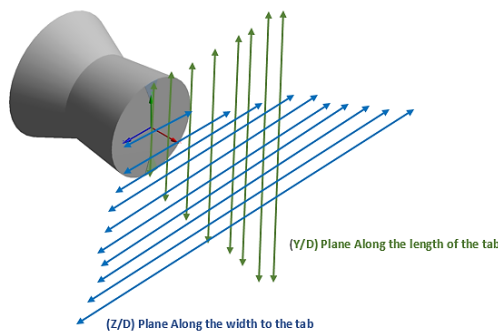


Fig. 15. Isometric view of delta tab at nozzle outlet representing x, y, and z-axes.

The non-dimensionalized total pressure is plotted against the non-dimensionalized distance along tab-length (Y/D) and along tab-width (Z/D) for varying axial positions, as illustrated in Fig. 15. For the uncontrolled jet, the pressure profiles in the radial location are shown in Figs. 16, 18, and 20 for NPR 5, 6, and 7, respectively. At NPR 5, pressure profile for the axial positions of $X/D = 0.5, 1, 2, 3, 5, 8, 10, 15,$ and 20 along and normal to the direction of the delta tabs for the controlled jet are plotted in Fig. 17. Further, the pressure plot will be obtained for NPR 6 and 7 (Figs. 19 and 21). The total pressure is found to be dropped marginally at $X/D = 0.5$, and a similar trend is observed for axial locations up to $X/D = 5$ at NPR 5, which is a clear indication of supersonic acceleration. The non-dimensionalized total pressure drop at the jet centerline is found to be maximum at $X/D = 5$, revealing maximum jet speed at that point. Also, the pressure profile is increased gradually around the jet from $X/D = 0$ to $X/D = 2$, which illustrates subsonic acceleration. The total pressure is found to be gradually rising as the attention is shifted away from the jet-axis and beyond that, it gets almost constant and then starts decreasing gradually. It is also noticed that as the axial distance increases, the pressure drop shifts from sharp to gradual in nature. The magnitude of total pressure is found to be highest at $X/D = 0.5$, whereas the total pressure abates along the downstream of the nozzle. Moving to farstream distance, the non-dimensionalized total pressure around the jet centerline is about 0.25 i.e. $(P/P_0) = 0.25$, which is steady in magnitude suggesting the invariant zone of Mach number near the jet. Moreover, an intriguing notice is that the symmetric behaviour of pressure profile is observed around the jet centerline in case of an uncontrolled jet. It results due to poor domination of vortex in the jet flow.

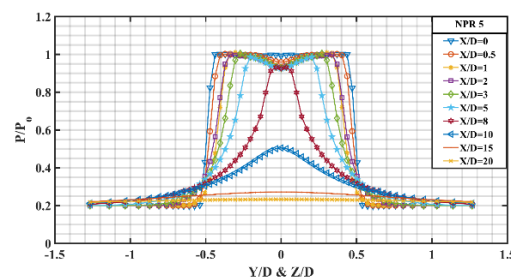
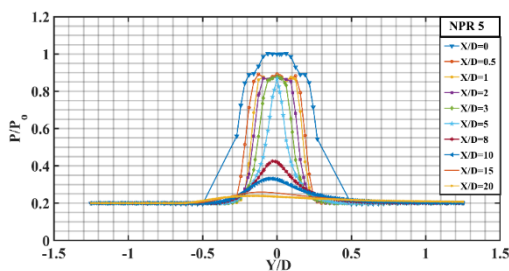


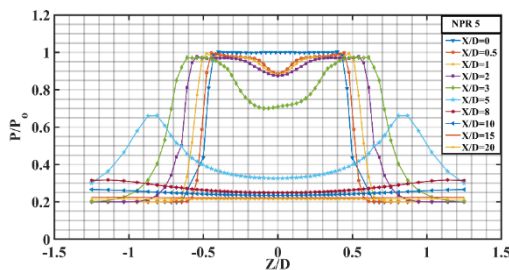
Fig. 16. Pressure profile of uncontrolled jet for NPR 5.

In case of the controlled jet regulated by delta tabs corresponding to NPR 5, which is a case of marginal overexpansion, pressure profiles are plotted for different axial locations at $X/D = 0, 0.5, 1, 2, 3, 5, 8, 10, 15$ and 20 in the directions along tab-length (Y/D) and along tab-width (Z/D) as shown in Figs. 17(a) and 17(b). There is hardly any noticeable drop in the pressure compared to that observed for the unrestrained jet at $X/D = 0.5$. The invariable pressure region in the near field region gets narrower as compared to the uncontrolled condition. It has also been found that in the controlled jet, there is a marginal pressure difference between axial positions

from $X/D = 0.5$ to $X/D = 5$ along the jet axis, as illustrated in Fig. 17(a). The constant pressure region reflects the mixing zone in the pressure profile, which is basically identical in both unconstrained and constrained jets. However, in case of the controlled jet, the region of rapid pressure drop is different from the uncontrolled jet. Moreover, it is also observed that there is an insignificant variation in the peak pressure at $X/D = 0.5, 1, 2, 3,$ and 5 along the tab which is a clear sign of momentum transfer due to delta tabs. The peak pressure is found to be reduced along the jet centreline in case of the controlled jet, which is a clear indication of weaker shock structures produced by the delta tabs. Also, it is seen that the pressure profiles get narrower in the direction along the tab as compared to the direction normal to the tab. Furthermore, higher jet spread can be observed in the direction along the tab. Two off-center pressure peaks are observed indicating jet bifurcation along the tab-length direction. Essentially, jet bifurcation helps in promoting the jet mixing. The pressure profile of unrestrained jet at NPR 6, which is a case of near correct expansion is shown in Fig. 18.



(a) Direction along tab-length (Y/D)



(b) Direction along tab-width (Z/D)

Fig. 17. Pressure profile of controlled jet for NPR 5.

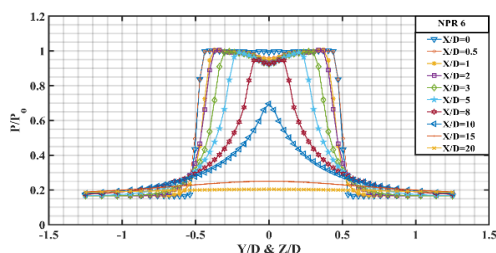
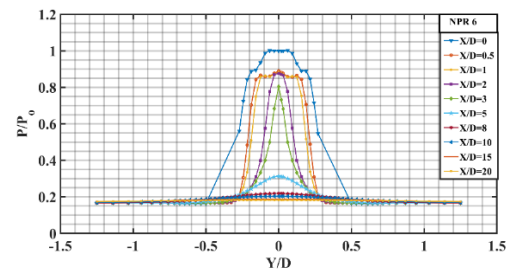
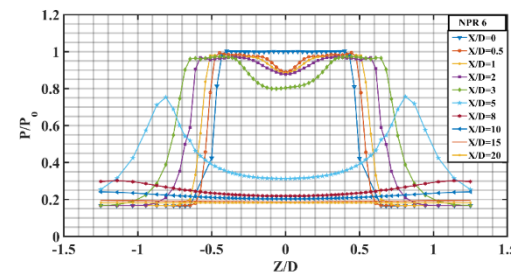


Fig. 18. Pressure profile of uncontrolled jet for NPR 6.

Pressure profiles observed for unrestrained jet corresponding to NPR 6 are similar to that at NPR 5. At $X/D = 0.5$, a slight drop in pressure along the jet centerline is observed indicating a rise in the velocity. Pressure gradually starts rising further along the radial direction indicating a reduction in velocity. The pressure starts decreasing as we move away from the nozzle outlet and it can be observed in the pressure profiles. The pressure rise is more at $X/D = 10$ for NPR 6 as compared to NPR 5 in case of the uncontrolled jet. It is fascinating to see that the pressure zone around the jet centerline corresponding to NPR 6 gets a little wider compared to NPR 5. Moreover, the pressure profiles around the far-field region ($X/D = 15$ and $X/D = 20$) for uncontrolled case is almost similar for both NPR 5 and NPR 6. Pressure profiles for the constrained jet corresponding to NPR 6 along tab-length (Y/D) and along tab-width (Z/D) are illustrated in Figs. 19(a) and 19(b), respectively.



(a) Direction along tab-length (Y/D)



(b) Direction along tab-width (Z/D)

Fig. 19. Pressure profile of controlled jet for NPR 6.

It is found that for controlled jet along the tabs at NPR 6, two off-center pressure peaks at $X/D = 0.5$ around the jet centerline drops, as compared to NPR 5. Also, the pressure profile zone beyond $X/D = 2$ gets narrower compared to the pressure zone for NPR 5. The narrowness of the pressure zone indicates the bounded velocity gradient between the fluid layers adjacent to the centerline. Further, it has been noticed that the marginal pressure variation which was present at NPR 5 for $X/D = 0.5, 1, 2, 3,$ and 5 is no longer prevalent for the same axial location at NPR 6. The magnitude of pressure peak varies and somewhat decreases for $X/D = 2, 3,$ and 5 for NPR 6. The decrease in the apex pressure at different axial locations for NPR 6, as compared to NPR 5, indicates an increase in the corresponding speed along the jet centerline as

a result of weak oblique shocks, present downstream to the nozzle exit. The two off-center pressure peaks along the tab-width direction (Z/D) clearly indicate jet bifurcation suggesting efficient mixing. Pressure profile for the unrestrained jet at NPR 7, which is a case of underexpanded jet is represented by Fig. 20. It is interesting to notice that, for axial locations of $X/D = 2, 3, 5, 8$ at NPR 7, the pressure at the jet centerline decreases significantly, when compared with NPR 6. On the other hand, at $X/D = 10$, there is an increase in pressure along the jet centerline at NPR 7 indicating an augmentation in shock-strength. Beyond $X/D = 10$, no significant variation is observed in the pressure profile.

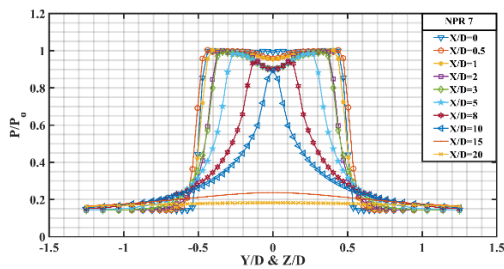
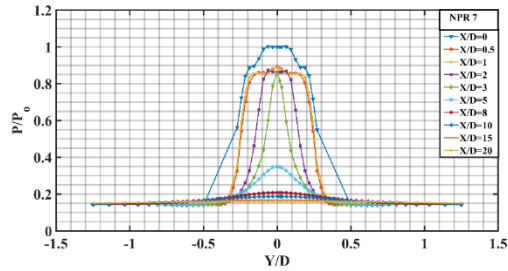


Fig. 20. Pressure profile of uncontrolled jet for NPR 7.

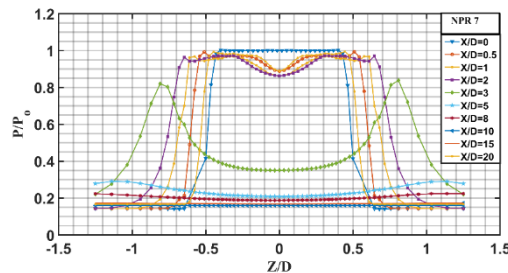
Pressure profile of controlled jet corresponding to NPR 7 which is a case of underexpanded jet is represented by Fig. 21(a) and Fig. 21(b). The off-center peaks for axial locations of $X/D = 0.5$ and $X/D = 1$ seems to have flattened a little, indicating a constant pressure zone for NPR 7. These flattened pressure profiles around the jet centreline show the significant influence of viscous action on the flow. Also, the pressure peak at $X/D = 3$ gets higher as compared to the pressure peak at NPR 6. Along tab-width direction (Z/D), at $X/D = 0.5, 1, 2, 3$, a suggestive abatement in the pressure indicating an increase in the supersonic acceleration at higher NPRs is observed. It is interesting to notice that at NPR 7, the bifurcation is spotted at $X/D = 3$ whereas, the same is spotted at $X/D = 5$ for NPR 6. Furthermore, the flow attains a self-similar zone beyond $X/D = 10$.

3.4 Mach Contour

The qualitative information related to the Mach number variation along the downstream-direction of the flow was plotted for the uncontrolled as well as controlled streams for different NPRs, as discussed below from Figs. 22 to 31. There are six prominent shock-cell structures along the downstream of the flow, which can be clearly observed in the contours representing Mach variation for the uncontrolled jet at NPR 4 as illustrated in Fig. 22. Figure 23(a) reveals that there has been a decrement in the number of shock-cell structures observed in the case of the controlled jet in the x - y plane at NPR 4. Figure 23(b) indicates the weakening of the shock strength in the x - z plane.



(a) Direction along tab-length (Y/D)



(b) Direction along tab-width (Z/D)

Fig. 21. Pressure profile of controlled jet for NPR 7.

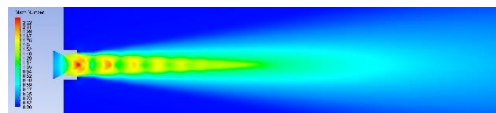
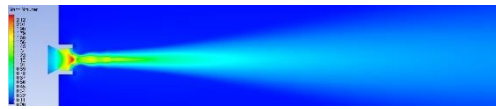
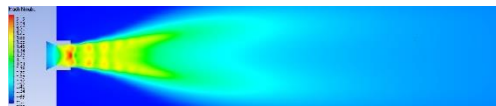


Fig. 22. Mach contour of unconstrained jet for NPR 4.



(a) Mach contour in the x - y plane



(b) Mach contour in the x - z plane

Fig. 23. Mach contour of constrained jet for NPR 4.

Moreover, elongation in the length of shock cells and the acuteness in jet core clearly indicates the strengthening of the oblique shock at NPR 5, as shown in Fig. 24. Also, a significant reduction in the number of shock cells in the controlled jet in the x - y plane at NPR 5 is observed, and interestingly, shocks get bifurcated indicating enhanced mixing due to delta tabs (Fig. 25).

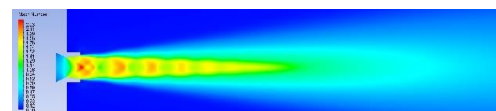
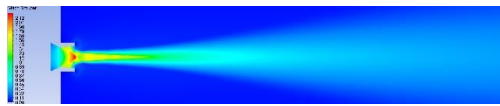
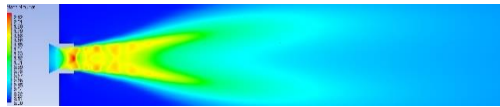


Fig. 24. Mach contour of unconstrained jet for NPR 5.

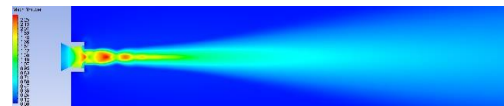


(a) Mach contour in the x-y plane

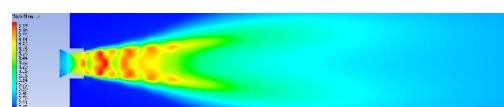


(b) Mach contour in the x-z plane

Fig. 25. Mach contour of constrained jet for NPR 5.



(a) Mach contour in the x-y plane



(b) Mach contour in the x-z plane

Fig. 29. Mach contour of constrained jet for NPR 7.

The shock cell structure for uncontrolled jet seems to be acquiring a diamond-like shape at NPR 6 as shown in Fig. 26. The fifth shock appears clearly at NPR 6, indicating an increase in the shock strength which was not distinct for lower NPRs. For controlled jet at NPR 6, the number of shocks decreases but these shock cells get more intense. Also, the two sharp arches in the x-z plane for controlled jet can be precisely observed in Fig. 27(b) indicating jet bifurcation, and this was not observable at lower NPRs.

From Fig. 30, it is found that the first shock appears to be more dominant and elongated than the subsequent shock-structures for the uncontrolled jet at NPR 8. Ultimately, an integrated effect of expansion at underexpanded condition and relaxation effect for controlled jet enlarges the shock from the exit of the nozzle at NPR 8 indicated by Fig. 31. Jet bifurcation is clearly observed in Fig. 31(b) and the first shock appears to be slightly dominant whereas the subsequent shocks are indistinct at NPR 8.

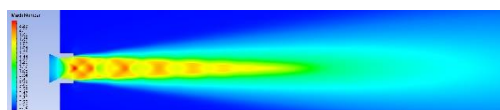


Fig. 26. Mach contour of uncontrolled jet for NPR 6.

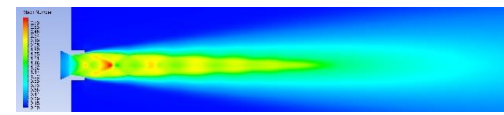
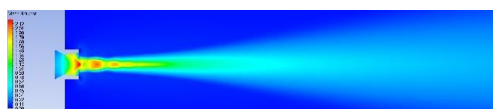
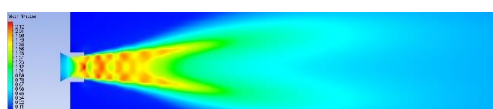


Fig. 30. Mach contour of uncontrolled jet for NPR 8.

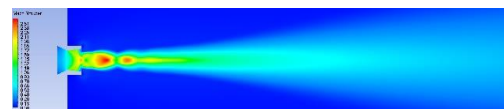


(a) Mach contour in the x-y plane

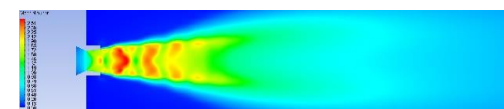


(b) Mach contour in the x-z plane

Fig. 27. Mach contour of constrained jet for NPR 6.



(a) Mach contour in the x-y plane



(b) Mach contour in the x-z plane

Fig. 31. Mach contour of constrained jet for NPR 8.

It is observed that the strength of shock decreases marginally for the uncontrolled condition of the jet at NPR 7 which is represented by Fig. 28 and it is almost similar to the contour at NPR 6. Furthermore, the shock gets stronger in case of the constrained jet at NPR 7 in comparison to the shock strength at low NPRs as can be seen in Fig. 29. Better visualization of the jet spread along with jet bifurcation is observed in Fig. 29(b).

3.5 Numerical Schlieren

The shock cell structure and the waves predominating in the flow-field for an unconstrained and constrained jet have been computationally generated using the numerical Schlieren image technique. The numerical Schlieren images qualitatively envisage the density variation of the fluid in the flow field. These images provide similar information as proclaimed by earlier experimental findings. All Figs. 32 to 41 illustrates a different pattern of shock-cell structure, which belongs to unconstrained and constrained jets

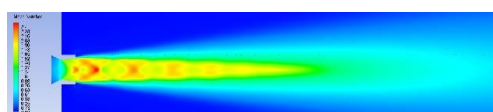


Fig. 28. Mach contour of uncontrolled jet for NPR 7.



Fig. 32. Numerical Schlieren of uncontrolled jet for NPR 4.



(a) x-y plane



(b) x-z plane

Fig. 33. Numerical Schlieren of controlled jet for NPR 4.

Furthermore, the comparison of Schlieren images at different NPRs implies a reduction in the number of shocks for the controlled jet suggesting the weakening of shocks by delta tabs. It is interesting to notice a shrinkage in jet core length for controlled jet implying faster centreline pressure decay and rapid mixing. Also at NPR 5, bifurcation of the jet can be clearly observed in Fig. 35(b), reaffirming the earlier inferences of efficient mixing.



Fig. 34. Numerical Schlieren of uncontrolled jet for NPR 5.



(a) x-y plane



(b) x-z plane

Fig. 35. Numerical Schlieren of controlled jet for NPR 5.



Fig. 36. Numerical Schlieren of uncontrolled jet for NPR 6.



(a) x-y plane



(b) x-z plane

Fig. 37. Numerical Schlieren of controlled jet for NPR 6.



Fig. 38. Numerical Schlieren of uncontrolled jet for NPR 7.

Furthermore, the bifurcated shock cell structure is found to be enlarged as compared with the earlier shock-cell structure of controlled jets at lower NPRs. The positive pressure gradient is responsible for the generation of expansion waves and when these waves combine with the relaxation effect, it happens to be the root cause of an enlarged bifurcated shock-cell structure at higher NPRs.



(a) x-y plane



(b) x-z plane

Fig. 39. Numerical Schlieren of controlled jet for NPR 7.



Fig. 40. Numerical Schlieren of uncontrolled jet for NPR 8.



(a) x-y plane



(b) x-z plane

Fig. 41. Numerical Schlieren of controlled jet for NPR 8.

4 CONCLUSIONS

This current numerical analysis endeavors to evaluate the efficacy of diametrically opposite axis-symmetric delta tabs in enhancing the jet mixing, located at the periphery of a convergent-divergent nozzle outlet (Mach number 1.8) with various levels of expansion. The numerical outcomes are found to be explicitly allied with the earlier published experimental results from the literature. Grid independent tests have been conducted and found, all the present results are independent of a grid size of over 2.1 million.

Interestingly, successive elongation has been observed, in the jet core length, for both unconstrained and constrained jets with increasing NPRs as a result of abated adverse pressure gradient. Further, the shock cell numbers are decreased for the controlled jet as compared to the uncontrolled jet. The reason can be attributed as the vortices shed by delta tabs which are of mixed-sized nature are responsible for weakening the strength of shock-cell structures.

Also, faster centreline pressure descent of jet, regulated with delta tabs, indicates the rapidity of the mixing process for the constrained cases in comparison with the unconstrained ones. Specifically, the highest decrement in core length of 70.81% is obtained for the constrained jet corresponding to NPR 6 (correctly-expanded). However, a further increase in NPR of the controlled jet provides an increasing trend in the core length. This signifies that the delta tabs perform better in overexpanded conditions. Furthermore, for controlled jets, the spreading rate is more at higher NPRs.

Two off-center peaks in pressure profile around the jet axis clearly indicate that the jet bifurcates into two individual sharp jets and that specifies efficient mixing.

The numerical schlieren images clearly reveal the strong compression waves prevailing at the nozzle outlet, constrained with delta tabs, at NPR 4 and NPR 5. Moreover, the numerical Schlieren images helped in visualizing stronger expansion fans formed at higher NPRs because of the combined effect of positive pressure gradient and relaxation effect, which was absent at lower NPRs.

ACKNOWLEDGMENTS

The authors profoundly recognize the Indian Institute of Technology Kharagpur for resolving the availability of computational resources, which enormously aided in concluding the present investigation.

REFERENCES

Acarer, S. (2020). Peak lift-to-drag ratio enhancement of the DU12W262 airfoil by

passive flow control and its impact on horizontal and vertical axis wind turbines. *Energy*, 117659.

Ahuja, K. K. and W. H. Brown (1989). *Shear Flow Control by Mechanical Tabs*, AIAA Paper, Tempe, AZ, U.S.A.

Behrouzi, P. and J. J. McGuirk (2006). Effect of Tab Parameters on Near-Field Jet Plume Development. *Journal of Propulsion and Power* 22, 576-585.

Bradbury, L. J. S. and A. H. Khadem (1975). The Distortion of a Jets by Tabs. *Journal of Fluid Mechanics* 70, 801-813.

Chin, C., M. Li., C. Harkin., T. Rochwerger., L. Chan., A. Ooi., A. Risborg and J. Soria (2013). Investigation of the Flow Structures in Supersonic Free and impinging Jet Flows. *Journals of Fluid Engineering* 135, 031202 1-15.

Ebrahimi, A. and M. Movahhedi (2018). Wind turbine power improvement utilizing passive flow control with microtab. *Energy* 150, 575-582.

Favre, A. (1969). Statistical equations of turbulent gases. In Problems of Hydrodynamics and Continuum Mechanics. *Philadelphia, SIAM*, 231-266.

Gatski, T. B. and J. P. Bonnet (2009). *Compressibility, Turbulence and High Speed Flow*, Elsevier: Amsterdam.

Gross, N., G. A. Blaisdell and S. Lyrintzis (2010). Evaluation of Turbulence Model Corrections for Supersonic Jets using the Overflow Code, *40th Fluid Dynamics Conference*, Chicago, Illinois.

Hirsch, C. (1990). *Numerical Computation of Internal and External Flows*, Vol. 2, John Wiley & Sons: Chichester.

Hussain, F.A.K.M. (1986). Coherent Structures and Turbulence. *Journal of Fluid Mechanics* 173, 303-356.

Kaushik, M. (2019). *Theoretical and Experimental Aerodynamics*, Singapore: Springer Nature.

Kaushik, M. and E. Rathakrishnan (2013). Corrugated Limiting Tab for Jet Mixing. *International Journal of Turbo and Jet-Engines* 30, 359-373.

Kaushik, M. and E. Rathakrishnan (2015). Tab Aspect Ratio Effect on Supersonic Jet Mixing. *International Journal of Turbo and Jet Engines* 32, 265-273.

Kaushik, M., K. Rakesh and G. Humrutha (2015). Review of Computational Fluid Dynamics Studies on Jets. *American Journal of Fluid Dynamics* 5, 1-11.

Maruthupandiyam, K and E. Rathakrishnan (2018). Shifted Triangular Tabs for Supersonic Jet

- Control. *Journal of Aerospace Engineering* 31 (5), 04018067.
- Medeiros, R. B., J. M Fusco., K. Ropelato and G. Aliatti (2014). Simulation of supersonic flow comparison of LES against URANS and RANS turbulence models, *10th world congress on computational mechanics*.
- Pope, S. B (1978). An explanation of round jet/ plane jet anomaly. *AIAA Journal* 16, 279-281.
- Ranjan, A., M. Kaushik., D. Deb., V. Muresan and M. Unguresan (2020), Assessment of Short Rectangular-Tab Actuation of Supersonic Jet Mixing. *Actuators* 2020,9,72.
- Samimy, M., M. Reeder and K. B. M. Q. Zaman (1991). *Supersonic Jet Mixing Enhancement By Vortex Generations*, AIAA Paper, Sacramento, CA, U.S.A.
- Steffen, C. J., D. R. Reddy and K. B. M. Q. Zaman (1997). *Numerical Modeling of Jet Entrainment for Nozzles Fitted with Delta Tabs*, AIAA Paper, Reno, NV, U.S.A.
- Thillaikumar, T., P. Bhale and M. Kaushik (2020). Experimental Investigations on the strut Controlled Thrust Vectoring of a Supersonic nozzle. *Journal of Applied fluid Mechanics* 13, 1223-1232.
- Tide, P. S. and V. Babu (2008). *A comparison of predictions by SST and Wilcox κ - ω Models for a Mach 0.9 Jet*, 46th AIAA Aerospace Science Meeting and Exhibit, Reno, Nevada.
- Wang, H., B. Zhang, Q. Qiu and X. Xu (2017), Flow control on the NREL S809 wind turbine airfoil using vortex generators. *Energy* 118, 1210-1221
- Zaman, K. B. M. Q. (1993). *Streamwise Vorticity Generation and Mixing Enhancement in Free Jets by Delta-Tabs*, AIAA Paper, Orlando, FL, U.S.A.
- Zaman, K. B. M. Q., M. F. Reeder and M. Samimy (1992). *Supersonic jet Mixing Enhancement by Delta-Tabs*, AIAA Paper, Nashville, TN, U.S.A.